### **ORGAN REGENERATION**

# A population of stem cells with strong regenerative potential discovered in deer antlers

Tao Qin¹†, Guokun Zhang²†, Yi Zheng³†, Shengyou Li³†, Yuan Yuan¹†, Qingjie Li⁴†, Mingliang Hu¹, Huazhe Si⁵, Guanning Wei⁶, Xueli Gao¹, Xinxin Cui¹, Bing Xia³, Jing Ren², Kun Wang¹, Hengxing Ba², Zhen Liu², Rasmus Heller³, Zhipeng Li⁵\*, Wen Wang¹, Jinghui Huang³\*, Chunyi Li².9\*, Qiang Qiu¹\*

The annual regrowth of deer antlers provides a valuable model for studying organ regeneration in mammals. We describe a single-cell atlas of antler regrowth. The earliest-stage antler initiators were mesenchymal cells that express the paired related homeobox 1 gene (*PRRX*1<sup>+</sup> mesenchymal cells). We also identified a population of "antler blastema progenitor cells" (ABPCs) that developed from the *PRRX*1<sup>+</sup> mesenchymal cells and directed the antler regeneration process. Cross-species comparisons identified ABPCs in several mammalian blastema. In vivo and in vitro ABPCs displayed strong self-renewal ability and could generate osteochondral lineage cells. Last, we observed a spatially well-structured pattern of cellular and gene expression in antler growth center during the peak growth stage, revealing the cellular mechanisms involved in rapid antler elongation.

ower vertebrates have a remarkable capacity to heal in a scar-free manner and regenerate lost appendages, even at the adult stage (1-5). By contrast, mammals have largely lost the capacity for appendage or organ regeneration (6). However, deer antler offers a singular model to study spontaneous regeneration in mammals because its regeneration is similar and clinically relevant to mammalian long-bone development (7-9). Every year in early spring, hard antlers are cast from their pedicles, then both antler bone and cartilage are regenerated from the pedicle periosteum located in the pedicle stumps. In late spring and early summer, antlers grow and calcify in about 3 to 4 months with a growth rate of 2.75 cm/day and a mineral apposition rate of 3.2 µm/day, the highest among medium- to large-sized mammals (10, 11). At the end of the summer, the antlers lose their velvet skin cover, leaving dead bone ready for fighting during the rut. Antlers are cast in the next spring, and then a new round of their regeneration starts. Studies on antler regeneration have

mainly focused on histological (12) and morphological (13) aspects of the regeneration process. Previous findings identified some positively selected genes, regulatory elements, and highly expressed genes associated with rapid antler growth (14), but the detailed cellular and molecular mechanisms involved in antler regeneration remain unclear.

To address this fundamental question, we set out to investigate in detail the cellular composition and gene expression dynamics of antler tissue throughout its regeneration cycle using single-cell transcriptome sequencing (scRNA-seq), then used in vivo and in vitro experiments to assess the potency and functionality of key populations of stem cells.

### Single-cell transcriptomic atlas of antler regeneration

During antler regeneration, cartilage and bone are fully regenerated annually at a rapid rate (11). To comprehensively assess the gene transcription dynamics and cell type changes that occur during antler regeneration, we applied scRNA-seq of sika deer (Cervus nippon) antlers at various stages of the regeneration process (10 days before casting, and 0, 2, 5, 10, 45, 60, and 90 days after casting) (Fig. 1A and fig. S1, A and B) (15). To ensure the accuracy and reliability of the subsequent analysis, we generated a chromosome-level genome assembly of a male sika deer (fig. S2 and tables S1 and S2), providing a solid foundation for the scRNA-seq analysis.

In total, we analyzed 74,730 cells covering the critical stages of antler regeneration (Fig. 1B and table S2). Cells from all samples were pooled and visualized so that the cells could be assigned to eight putative cell populations (Fig. 1B). These populations (associated markers in parentheses) are *PRRXI*<sup>+</sup> mesenchymal cells (PMCs; *PRRXI*, *POSTN*, and *LUM*), *SOX9*<sup>+</sup> chondroblasts (*SOX9* and *SOX6*), *PHEX*<sup>+</sup> osteoblasts

(PHEX), COL3A1<sup>+</sup> fibroblasts (COL3A1 and COL12A1), CHAD<sup>+</sup> chondrocytes (CHAD, SCRG1), ACTA2<sup>+</sup> pericytes (ACTA2 and MYLK), PECAM1<sup>+</sup> endothelial cells (PECAM1 and VWF), and PTPRC<sup>+</sup> immune cells (PTPRC and LCP1) (Fig. 1D and table S3). Of these, PMCs were particularly abundant in the samples (fig. S1, C and D). Cells of this type are reportedly crucial during limb regeneration in frog (16) and axolotl (2), as well as digit tip regeneration in mouse (17), supporting a key role in antler regeneration.

Next, we explored the lineage relationships among cell subtypes (Fig. 1C and fig. S1E) (15). This regeneration trajectory was dominated by PMCs, chondroblasts, and chondrocytes, with a general trend of progressive change from PMCs to chondroblasts and chondrocytes (Fig. 1C). Concomitantly, genes highly expressed in PMCs (such as POSTN and PRRXI) were gradually down-regulated, whereas characteristic genes in chondroblasts (such as SOX6) and chondrocytes (for example, CHAD, ACAN, and COL2AI) were up-regulated upon terminal differentiation (Fig. 1C). The samples from 10 days before casting and 0 days after casting had a highly similar cell composition, and PMCs were already present in the periosteum at the preregeneration time point (10 days before casting), suggesting that PMCs are permanently present in the antlergenerating tissues and are not formed by dedifferentiation (fig. S1B). This is in sharp contrast to the process observed in axolotl limb regeneration (2), in which the PRRXI<sup>+</sup> cell population first undergoes dedifferentiation to form progenitor cells and subsequently redifferentiates to form a PRRXI+ cell population. The reconstructed regeneration trajectory suggests that the annual cycle of antler regeneration is based on PMCs, in accordance with the notion that organ regeneration is a stem cell-based process in mammals (6, 18).

### Cell population dynamics during antler regeneration

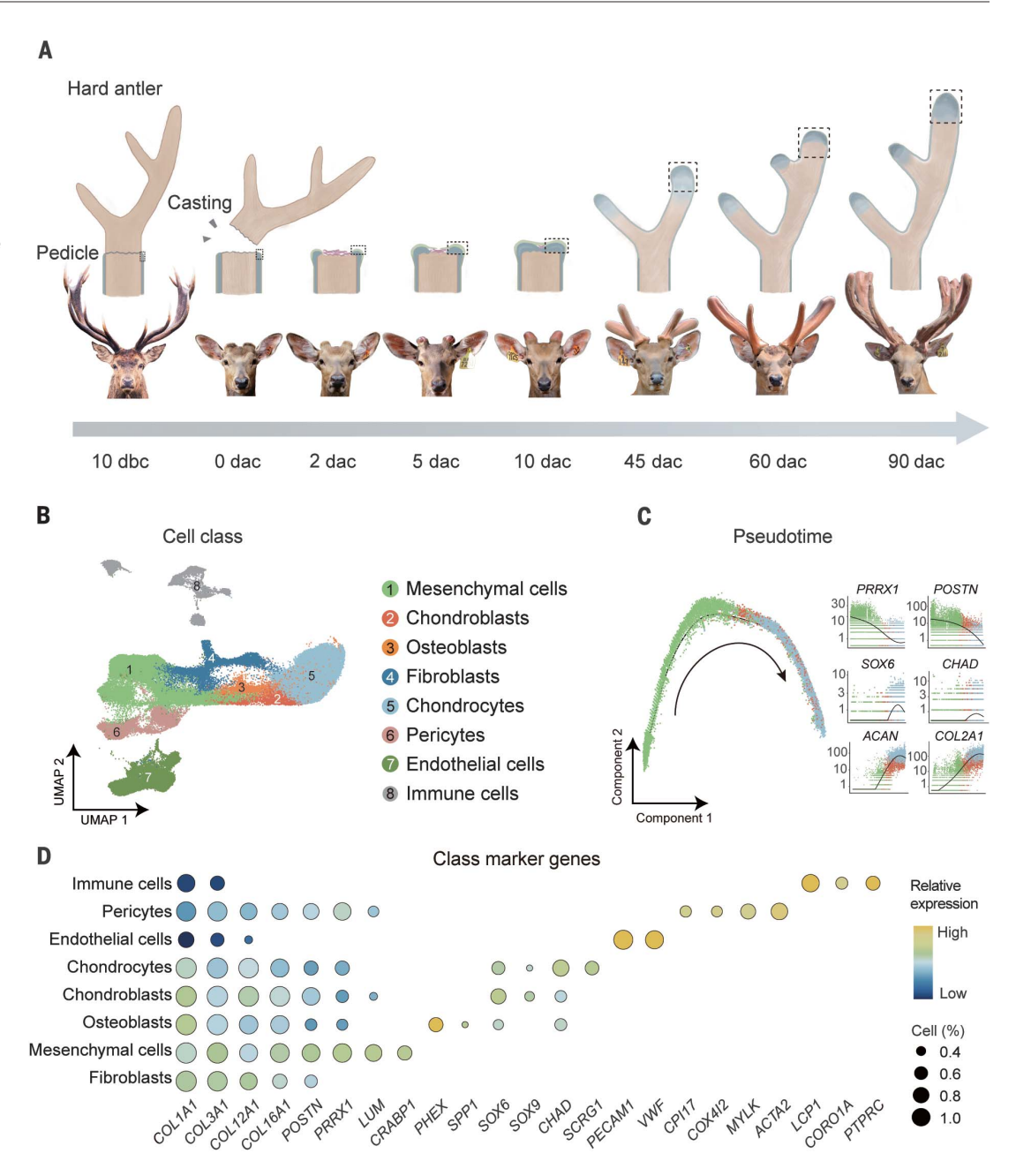
To analyze the osteochondral regeneration process in detail, we performed a subclassification analysis of the annotated cell types (Fig. 2A, fig. S3A, and table S3). As described above, in the pedicle periosteum at 10 days before casting (preregeneration) and 0 days after casting, the PMCs were abundant and represented a major periosteal cell population (Fig. 2B and fig. S3B), appearing to be the key cells for antler osteochondral regeneration. We thus analyzed the cellular composition of PMCs and found three subtypes: periosteal stromal cells (SFRP2+ cell population; PMC1), periosteal mesenchymal progenitor cells (PMF1+ cell population; PMC2), and chemotactic periosteal cells (CXCL14+ cell population; PMC3) (Fig. 2A). These cells were immunohistochemically confirmed to reside simultaneously in the pedicle periosteum (fig. S3C).

\*Corresponding author. Email: qiuqiang@lzu.edu.cn (Q.Q.); lichunyi1959@163.com (C.L.); huangjh@fmmu.edu.cn (J.H.); wenwang@nwpu.edu.cn (W.W.); zhipengli@jlau.edu.cn (Z.L.) †These authors contributed equally to this work.

Qin et al., Science **379**, 840–847 (2023) 24 February 2023

<sup>&</sup>lt;sup>1</sup>School of Ecology and Environment, Northwestern Polytechnical University, Xi'an 710072, China. <sup>2</sup>Institute of Antler Science and Product Technology, Changchun Sci-Tech University, Changchun, China. <sup>3</sup>Department of Orthopaedics, Xijing Hospital, Fourth Military Medical University, Xi'an 710032, China. <sup>4</sup>Research Center of Traditional Chinese Medicine, The Affiliated Hospital to Changchun University of Chinese Medicine, Changchun 130021, China. <sup>5</sup>College of Animal Science and Technology, Jilin Agricultural University, Changchun, China. <sup>6</sup>School of Life Sciences, Jilin University, Changchun 130012, Jilin, China. <sup>7</sup>Section for Computational and RNA Biology, Department of Biology, University of Copenhagen, N 2200 Copenhagen, Denmark. <sup>8</sup>Center for Excellence in Animal Evolution and Genetics, Chinese Academy of Sciences, Kunming 650223, China. <sup>9</sup>College of Traditional Chinese Medicine, Jilin Agricultural University, Changchun China

Fig. 1. An integrated developing cell atlas of regenerating antlers. (A) Schematic of the workflow of scRNA-seq-based antler regeneration analysis, using samples collected from sites (outlined with black dotted lines) during indicated phases of the process. dbc, days before casting; dac, days after casting. (B) Uniform manifold approximation and projection (UMAP) atlas of color-coded cell classes involved in antler regeneration based on the scRNA-seg data. (C) (Left) Developmental trajectory of PRRX1+ mesenchymal cells (PMCs) to chondroblasts and chondrocytes inferred by Monocle 2 and colored by cell clusters (left panel). (Right) Plots showing the relative expression of differentially expressed genes in pseudotime order. Each dot indicates a single cell, with color coding showing cell clusters. (D) Dot plot showing cell class-level marker gene expression.



In addition to the three mesenchymal subtypes detected at 10 days before casting and 0 days after casting, another type of PMC (denoted PMC4, expressing TNN), as well as small proportions of chondrogenic cells, were observed at 5 days after casting (Fig. 2B), indicating that cellular heterogeneity had increased and chondrogenic differentiation had begun by 5 days after casting. Because PMCs were abundant at both 0 and 5 days after casting (Fig. 2B), we compared the ability of cell masses at these two points to generate antlers ectopically in nude mice (15). In contrast to cell masses at 0 days after casting, which generated fibrous connective tissue, cell masses at 5 days after casting successfully differentiated into an antler-like structure (with cartilage and bone) by 45 days after transplantation (Fig. 2C and fig. S4A), confirming their ectopic antler generation capacity. We further transplanted cell masses at 5 days after casting into the heads of tdTOMATO (red fluorescent protein)-labeled nude mice. No red fluorescence was visualized in the regenerated cartilage and chondrocytes (fig. S5A), and the singlecell atlas showed that the chondrocytes did not express the tdTOMATO (fig. S5, B and C), confirming that the regenerated cartilage was derived from the tissue transplanted 5 days after casting and not from the host cells. The PMC4 cells at 5 days after casting highly expressed multiple genes that support regeneration, including *PTN*, *TNC*, *TNN*, and *DLX5*, which are associated mainly with chondrogenesis and limb development (Fig. 2, D and E, and fig. S4). A pseudotime analysis showed that regenerating cartilage in both antlers and nude mouse heads was formed by differentiation of PMC4 (fig. S4E and fig. S5, D and E) (15), corroborating that they are the key cell population for antler regeneration.

We further delineated the origin of the PMC4 cell population. Because PMC1, PMC2, and PMC3 were present at earlier time points (10 days before casting and 0 days after casting) than PMC4 (5 days after casting), we initially compared the transcriptomic similarities of PMC4 to other PMCs. The gene expression

Qin et al., Science 379, 840-847 (2023) 24 February 2023 2 of 8

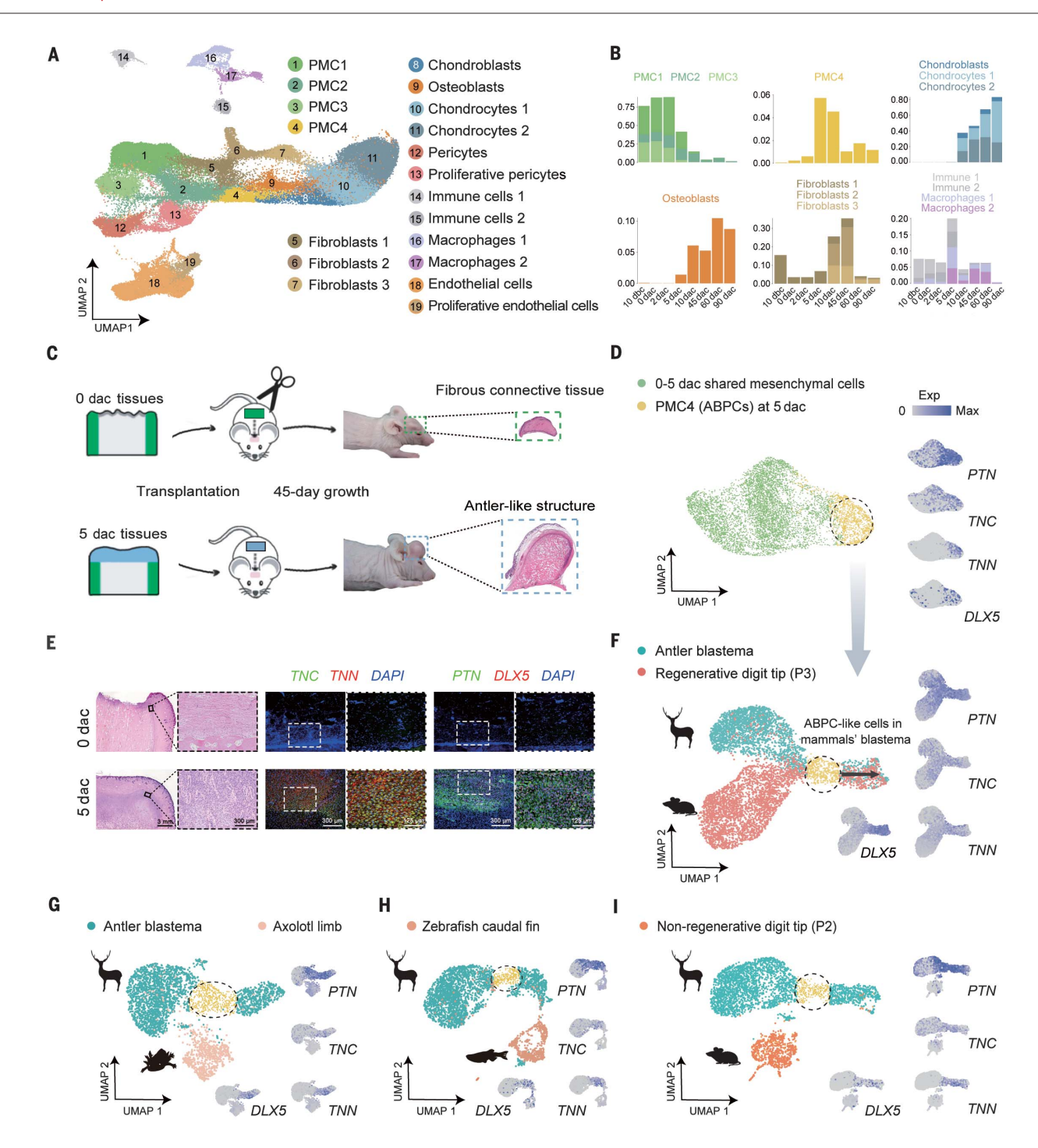
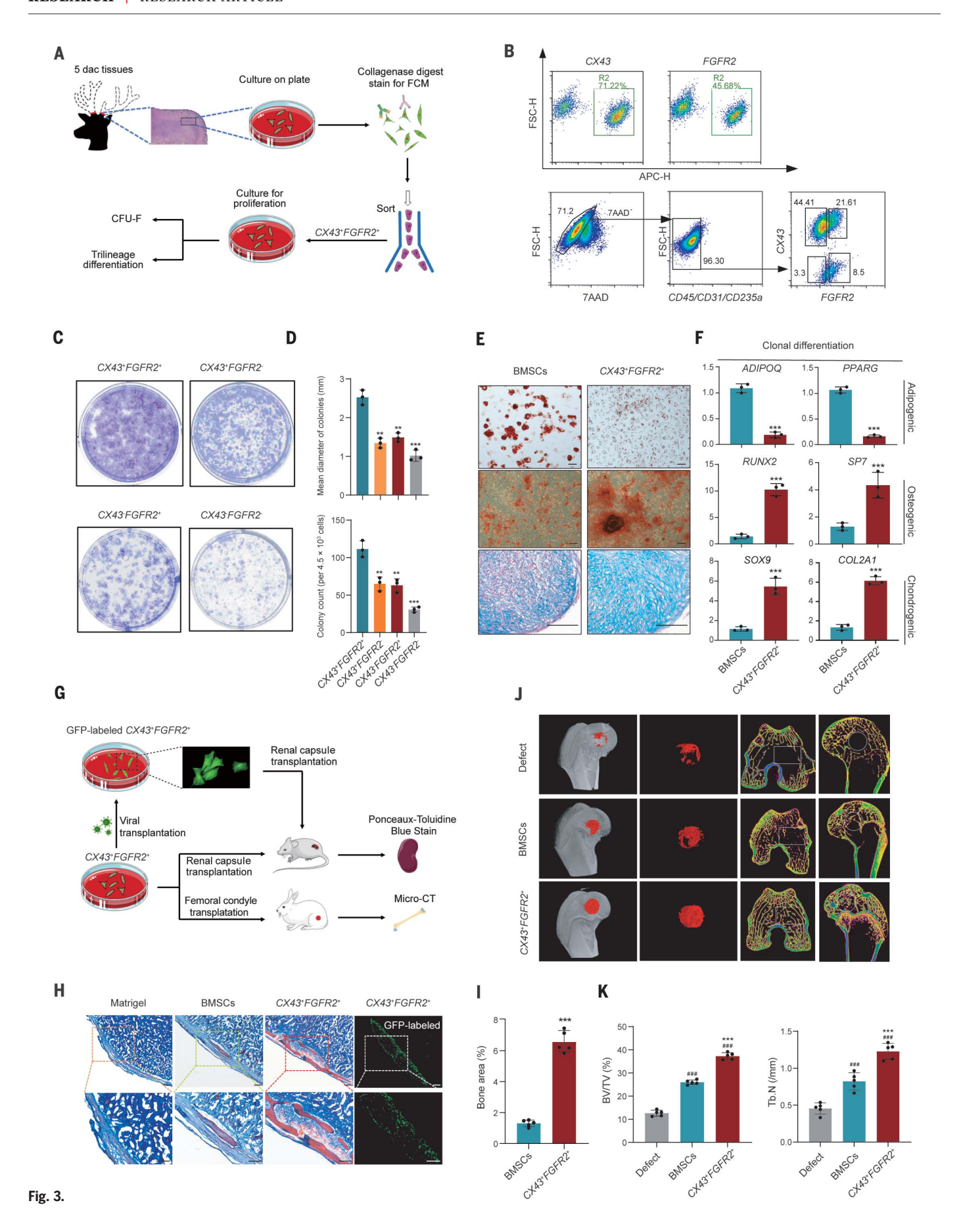


**Fig. 2. Cellular dynamic atlas of antler regeneration and identification of critical regenerative progenitor cells.** (**A**) UMAP atlas of antler regeneration with color-coded cell types, annotated by means of scRNA-seq analysis of cell-lineage specific markers. (**B**) Proportions of cell types at indicated time points. (**C**) Schematic illustration of ectopic antler-generation assays. Cell masses collected at 0 and 5 days after casting were transplanted onto heads of nude mice. The former remained fibrous connective tissue, but the latter had differentiated into an antler-like structure by 45 days after transplantation. (**D**) UMAP atlas based on scRNA-seq data of mesenchymal cells present in tissues sampled at 0 to 5 days after casting (green) and PMC4 [defined as antler blastema progenitor cells (ABPCs)] specifically expressed in tissues sampled at 5 days after casting (yellow). Feature plots to the right (blue) visualize expression of PMC4 marker genes (*PTN*, *TNC*, *TNN*, and *DLX5*).

**(E)** Longitudinal sections of (top) pedicle periosteum at 0 days after casting and (bottom) regenerating antler tissues at 5 days after casting, stained with hematoxylin and eosin and selective marker genes. The boxed areas correspond to the higher-magnification views. **(F)** UMAP atlas based on integrated single-cell analysis of antler blastema (blue) and mouse regenerative digit tip (P3) (red). ABPC-like cells are circled with a dashed line. The arrow indicates the differentiation direction of ABPC-like cells toward osteochondral cells. Feature plots to the right visualize expression of ABPC marker genes (*PTN*, *TNC*, *TNN*, and *DLX5*). **(G** to I) UMAP atlas based on (G) integrated single-cell analysis of antler blastema (blue) and axolotl limb (orange), (H) zebrafish caudal fin (orange), and (I) mouse nonregenerative digit tip (P2) (orange). ABPCs are circled with a dashed line. Feature plots to the right visualize expression of ABPC marker genes (*PTN*, *TNC*, *TNN*, and *DLX5*).

Qin et al., Science 379, 840-847 (2023) 24 February 2023 3 of 8



Qin et al., Science **379**, 840–847 (2023) 24 February 2023

**Fig. 3.** Phenotypic and functional characterization of ABPCs (*CX43*+*FGFR2*+ cells). (**A**) Experimental scheme of *CX43*+*FGFR2*+ cells isolation and characterization in vitro. (**B**) (Top) Flow cytometric analysis detected expression of *CX43* and *FGFR2* in ABPCs. (Bottom) Flow cytometry gating strategies for sorting *CX43*+*FGFR2*+ cells at 5 days after casting. (**C**) Representative crystal violet staining of fibroblast colony-forming unit (CFU-F) colonies from populations sorted with flow cytometry. (**D**) Numbers and mean diameters of the CFU-F colonies. \*\*P < 0.01; \*\*\*P < 0.001 versus *CX43*+*FGFR2*+ cells. (**E**) Representative (top) oil red O, (middle) alizarin red, and (bottom) alcian blue stainings after adipogenic, osteogenic, and chondrogenic differentiation of clonally expanded *CX43*+*FGFR2*+ cells and BMSCs. Scale bar, 100 μm. (**F**) Results of reverse transcription polymerase chain reaction analyses of adipogenic, osteogenic, and chondrogenic marker genes in clonally expanded

 $CX43^+FGFR2^+$  cells and BMSCs before and after in vitro differentiation. \*\*\*\*P < 0.001 versus BMSCs. (**G**) Experimental scheme of  $CX43^+FGFR2^+$  cells characterization in vivo. (**H**) Results of histological analysis of subcapsular xenografts 8 weeks after implantation of Matrigel, BMSCs,  $CX43^+FGFR2^+$  cells, and GFP-labeled  $CX43^+FGFR2^+$  cells in immunodeficient mice. Scale bar,  $100~\mu m$ . (**I**) Bone areas formed in renal subcapsular layers 8 weeks after implantation of  $CX43^+FGFR2^+$  cells and BMSCs. \*\*\*P < 0.001 versus BMSCs. (**J**) Results of micro-computed tomography analysis of femoral condyle defects repair by means of local transplantation of  $CX43^+FGFR2^+$  cells and BMSCs in rabbits. (**K**)  $CX43^+FGFR2^+$  cells achieved higher bone-volume fractions [bone volume/total volume (BV/TV)] and trabecular numbers (Tb.N) than that of BMSCs in repairs of femoral condyle defects in rabbit. \*\*#\*P < 0.001 versus Defect: \*\*\*P < 0.001 versus BMSCs.

profile of PMC4 showed higher correlation to PMC2 than to PMC1 and PMC3 (fig. S6A). The Gene Ontology functional enrichment results indicated that the highly expressed genes in PMC2 were involved mainly in skeletal system development (fig. S6B and table S4). The pseudotime analysis further identified a major trajectory from PMC2 to PMC4 (fig. S6) (15). In vivo lineage tracing of cell differentiation would provide further insights into this process, but carrying out such controlled experiments in a large wild animal is not possible. Overall, our data suggests that PMC2 might be a population of resting stem cells residing in the periosteum before regeneration, which becomes activated and starts to form PMC4 by 5 days after casting, when the antler regeneration process starts. Concomitantly, expression of the suppressor genes (SFRP1, SFRP2, and SFRP4) of the Wnt pathway declined, whereas expression of WNT5B, TGFBI, and TGFBI genes increased (fig. S6E). suggesting that the Wnt and TGFB pathways might be involved in PMC4 formation.

In addition, proliferating pericytes and endothelial cells (*TOP2A* and *MKI67*) were also found at 5 days after casting (fig. S3D), which could be related to formation of the vascular network involved in antler growth (*19*). We also observed a increase in macrophages (*CD86*), which are required for wound healing or epimorphic regeneration in mammals and amphibians, at 5 days after casting (Fig. 2B). This indicates that the immune system also plays an important role in antler regeneration, similar to its reported involvement in amphibian appendage regeneration (*20*).

The cell populations at 5 days after casting meet the definition of a blastema. This is a cell mass that, through migration and proliferation, transiently forms at an injury plane and is endowed with the morphogenetic information required to regenerate an organ (21). Because PMC4 was identified as the key cell population for antler regeneration, we refer to these cells as "antler blastema progenitor cells" (ABPCs). We further compared the cellular composition in the blastema across species [deer antler, mouse regenerative digit tip (distal phalanx, P3), axolotl limb, and zebrafish caudal

fin] using data from this and previous studies (fig. S7) (3, 22, 23). Although the blastema cell composition varies greatly among species, PRRX1<sup>+</sup> cells were the most abundant cell type across species. We identified several conserved marker genes, such as *POSTN* and *DCN*, which suggests a conserved core mechanism in the process of appendage regeneration (fig. S7G). We identified a specific subtype of *PRRXI*<sup>+</sup> cells in the mouse digit tip (P3) blastema with gene expression profiles similar to those of ABPCs but not to those of nonregenerative digit tip (middle phalanx, P2), axolotl limb, and zebrafish caudal fin blastema (Fig. 2, F to I; figs. S7 and S8; and tables S5 and S6). These findings indicate the potential existence of a cell population across mammals that is essential and specific for mammalian appendage regeneration.

We observed greater heterogeneity of cellular populations at 10 days after casting than at the earlier time points, with large proportions of ABPCs (4.53%), chondroblasts (6.75%), chondrocytes (30.78%), and osteoblasts (8.16%) (Fig. 2B). We also observed increases in the expression of chondrogenic genes such as SOX6, ACAN, and CHAD (fig. S3E), indicating that cartilage had developed rapidly by 10 days after casting. At 45, 60, and 90 days after casting, the proportion of chondrocytes and osteoblasts had increased further (Fig. 2B). Furthermore, expression of genes involved in ossification (PAPSS2, PHOSPHO1, and IBSP) had increased (fig. S3E), indicating that the endochondral ossification processes of antler development had started at this stage.

At this stage, we have focused mostly on the bone regeneration process in antler regrowth. However, antler regrowth also requires the proliferation of other cell types, such as the extracellular matrix of cartilage. Concordantly, we identified three fibroblastic cell clusters, denoted fibroblast 1, fibroblast 2, and fibroblast 3 (Fig. 2A and fig. S9A). During antler regeneration, we found that fibroblast 1 together with PMC2 were already present in periosteum before regeneration (10 days before casting) (Fig. 2B). Fibroblast 2 and 3 cells started to appear at 10 days after casting, were maintained at high levels during mid-regeneration stages (10 to

45 days after casting), and substantially declined during the antler ossification period (60 to 90 days after casting) (Fig. 2B). The pseudotime analysis showed a differentiation trajectory from fibroblast 1 to fibroblasts 2 and 3 (fig. S9B), which potentially secrete the large amounts of collagen needed to form the extracellular matrix of cartilage during antler regeneration.

## Phenotypic and functional characterization of ABPCs at 5 days after casting

ABPCs in the blastema at 5 days after casting play a crucial role in antler regeneration. We isolated ABPCs for further phenotypic and functional characterization (Fig. 3A). We identified a cluster of genes enriched in ABPCs (fig. S10A and table S7). Two cell surface markers (*CX43* and *FGFR2*) were highly and differentially expressed in ABPCs (Fig. 3B and fig. S10B). Subsequently, *CX43*\**FGFR2*\* ABPCs were sorted with flow cytometry for functional analysis (Fig. 3B).

The colonies formed by CX43<sup>+</sup>FGFR2<sup>+</sup> cells could clonally expand and be serially passaged, generating secondary and tertiary colonies that maintained the immunophenotypes, indicating their self-renewal ability. Moreover, these cells had a much higher colony-formation efficiency and generated much larger colonies than did CX43+FGFR2-, CX43-FGFR2+, and CX43-FGFR2 cells (Fig. 3, C and D). Next, we subjected clonal cultures to in vitro differentiation assays. The CX43<sup>+</sup>FGFR2<sup>+</sup> cells showed strong osteogenic and chondrogenic, but not adipogenic, differentiation capability (Fig. 3E and fig. S10C). This differs markedly from the trilineage differentiation of bone marrow stromal cells (BMSCs), currently the most widely used stem cells in bone regenerative medicine (24). In addition, under the same conditions, the CX43<sup>+</sup>FGFR2<sup>+</sup> cells showed stronger osteochondrogenic differentiation ability than did BMSCs, manifested by higher expression levels of osteogenesis markers (RUNX2 and SP7) and chondrogenesis markers (SOX9 and COL2A1) but not adipogenesis markers (ADIPOQ and PPARG) (Fig. 3F). Thus, deer antler CX43+FGFR2+ cells maintain selfrenewal capability and have strong potency

Qin et al., Science 379, 840–847 (2023) 24 February 2023 5 of 8

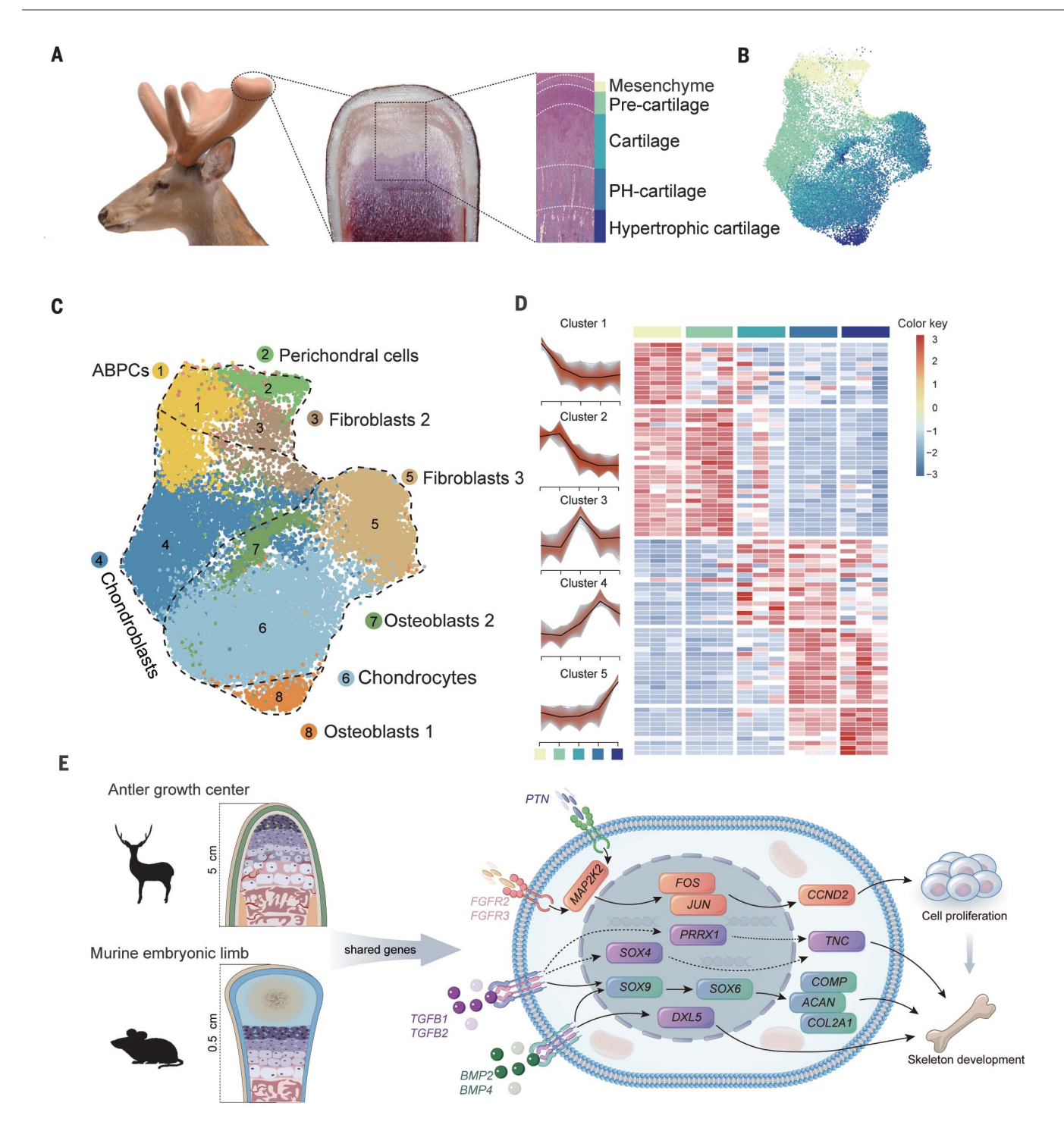


**Fig. 4.** Spatial cellular and genetic heterogeneity in rapid antler growth.

(A) (Left) Antler in the rapid growth period, with an antler growth center (AGC) circled by a dashed line. (Middle) The distinct AGC morphology. (Right) Histological section of AGC. (B) UMAP atlas of merged scRNA-seq data from mesenchyme layers, precartilage layers, cartilage layers, prehypertrophic cartilage layers (PH cartilage layers), and hypertrophic cartilage layers (n = 30,045 cells). Each

dot indicates a single cell and is colored according to its layers. ( $\mathbf{C}$ ) UMAP atlas of the AGC with color-coded cell-types identified with scRNA-seq analysis. ( $\mathbf{D}$ ) (Left) Fuzzy c-means clustering identifying general patterns of gene expression across the five tissue layers in AGC. (Right) Heatmap of gene expression levels from distal to proximal AGC cell layers. The gene details are shown in table S9. ( $\mathbf{E}$ ) Schematic diagram of shared highly expressed genes in AGC and mouse embryonic limb.

toward osteochondrogenic differentiation, highlighting their potential utility in cell-based therapy for bone and cartilage regeneration.

To further assess the in vivo differentiation potential of  $CX43^+FGFR2^+$  cells, we transplanted

cell cultures into renal capsules of immunodeficient mice (Fig. 3G). Eight weeks after transplantation, the  $CX43^+FGFR2^+$  cells showed a strong osteochondral differentiation capacity (Fig. 3H). They formed significantly greater areas of new cartilage and bone than did BMSCs (Fig. 3I). Furthermore, the regenerated cartilage and bone were derived from the *CX43*\**FGFR2*\* cells labeled with green fluorescence (Fig. 3H). To further assess their potential

Qin et al., Science 379, 840-847 (2023) 24 February 2023 6 of 8

therapeutic value in regenerative medicine and bone remodeling, CX43+FGFR2+ cells were used to repair femoral condyle defects in rabbit, with BMSCs as controls. After 8 weeks, both BMSCs and CX43+FGFR2+ cells had filled the cavities with newly formed bone, but the CX43<sup>+</sup>FGFR2<sup>+</sup> cells generated higher numbers of new trabecular bone (Fig. 3, J and K, and fig. S10). Thus, CX43<sup>+</sup>FGFR2<sup>+</sup> cells have a strong capacity to promote bone formation in vivo, with potential for cell-based therapies to promote bone regeneration (for example, for bone or cartilage injuries, nonunion fractures, and osteoporosis). In contrast to other stem cell types, CX43<sup>+</sup>FGFR2<sup>+</sup> cells have advantages including superior proliferative and osteochondral differentiation ability and ex vivo expansion. Nevertheless, we stress that many concerns about the use of deer CX43<sup>+</sup>FGFR2<sup>+</sup> cells in the clinic remain to be addressed in future studies, including their detailed molecular regulation mechanisms and the safety hazards involved in their use, as well as ethical and legal concerns.

# Spatial cellular and genetic heterogeneity during rapid antler growth

The rate of bone growth in deer antler is the highest recorded for any animal (10). The antler growth process is spatially well organized, with an antler growth center (AGC) forming at the antler tip (12) (Fig. 4A). The AGC becomes the primary growth center for rapid antler elongation and recapitulates the growth center of the embryonic long bone histologically (10). To characterize its spatial heterogeneity at cellular and gene expression levels, we applied scRNA-seq and bulk RNA-seq analyses to AGC tissue layers at 60 days after casting, around the time point when antlers grow most rapidly in sika deer (Fig. 4A and table S2).

The single-cell mapping matched the histological spatial location distribution (Fig. 4B, fig. S11A, and table S8). The mesenchyme layer at the most distal part of the antler tip was composed mainly of perichondral cells (29.68%) and ABPCs (49.96%) (Fig. 4, B and C, and fig. S11), suggesting that the ABPCs that formed by 5 days after casting persist at the tip as a stem cell pool for antler growth. The precartilage layer was dominated by chondroblasts (51.90%), which are key cells for chondrogenesis, and a smaller proportion of ABPCs (20.52%) (Fig. 4, B and C, and fig. S11). The cartilage and prehypertrophic cartilage (PH cartilage) layers were dominated by chondrocytes (61.47%) (Fig. 4, B and C, and fig. S11). The hypertrophic cartilage layers consisted mainly of osteoblasts (63.87%) (Fig. 4, B and C, and fig. S11), which is in line with the histological findings that hypertrophic cartilage is being replaced by spongy bone (10). The spatial heterogeneity of cell composition in the AGC was confirmed with histology (fig. S11). We reconstructed the spatial cellular atlas of the AGC from distal to proximal layers, expanding our understanding of the spatial locations of major cell populations during the rapid elongation of deer antler.

Next, we assessed the global variation in gene expression across the AGC tissue layers, using the bulk RNA-seq data (table S2). Principal components analysis (PCA) revealed a gradient of layer samples that matched their positions along a proximal-distal axis of the AGC (fig. S11E), suggesting that the gene expression variation trajectory follows a pattern similar to that found in the AGC tissue layers. Highly expressed genes in mesenchyme layers were found to be involved in cell proliferation (for example, IGF1, IGFBP2, and IGFBP4) and stem cell maintenance (such as SFRP1 and SFRP2) (Fig. 4D and table S9). This is expected because the rapid cell proliferation in antlers presumably requires factors that not only stimulate rapid cell proliferation but also maintain the stemness of ABPCs and control the cell cycle. Genes highly expressed specifically in the precartilage layers (for example, WNT10B, WNT10A, and WNT6) were associated with the Wnt pathway (Fig. 4D and table S9), suggesting that this signaling pathway could be involved in early differentiation of stem cells toward chondrogenesis. The highly expressed genes in the cartilage layers and PH cartilage layers were related to cartilage development (such as SOX6 and SOX9) and extracellular matrix organization (such as COL2A1) (Fig. 4D and table S9). The highly expressed genes in the hypertrophic cartilage layers were related to chondrocyte mineralization (such as MMP9 and MMP12) (Fig. 4D and table S9).

The histology of deer AGCs resembles the growth plates of developing long bone in mammals (10), suggesting that they may share similar growth mechanisms. To test this hypothesis, we reanalyzed the scRNA-seq profiles of mouse embryonic limbs and compared them with AGCs (25). We found that they shared 151 highly expressed genes (table S10) primarily related to extracellular matrix organization, skeletal system development, cartilage development, and cell proliferation (table S10). Several core genes of the mitogen-activated protein kinase (MAPK) signal pathway (FGFR2, FGFR3, MAP2K2, FOS, and JUN), bone morphogenetic protein (BMP) signal pathway (BMP2 and BMP4), and transforming growth factor-β (TGFβ) signal pathway (TGFB1 and TGFB2) were highly expressed in both AGCs and mouse neonatal growth plates (26, 27). The marker genes (PRRX1, TNC, DLX5, PTN, and SOX4) for ABPCs were also identified during rapid limb development in mice, suggesting potential roles of those genes for rapid skeleton development in mammals (Fig. 4E, fig. S11, and table S10). Moreover, we detected multiple angiogenesis-related genes (VAV3, ANGPTL2, MYH9, and ACTGI) in AGC (table S10), most likely related to the highly vascularized cartilage in deer antlers (19). This is a distinctive feature of antler growth, which differs sharply from the avascular chondrogenesis in mice and human tissues and serves the high metabolic demands of rapidly growing antler tissue (14).

#### Conclusion

We present a spatiotemporal cellular atlas of antler regeneration, which provides a useful genetic and histological resource for mammalian organ regeneration. Our results show that antler regeneration is consistent with a conceptual stem cell-based regenerative process. We provide evidence for the existence of a blastema-like structure that is present during antler regeneration and is similar to the structure involved in amphibian limb regeneration, suggesting that the blastema is a conserved biological feature in vertebrate tissue regeneration. We further identified a population of regenerative progenitor cells, ABPCs, in the antler blastema, with impressive capacities for self-renewal, osteogenic-chondrogenic differentiation, and bone-tissue repair. This provides a cellular basis for understanding antler regeneration and extends the catalog of known mammalian stem cell systems. Cross-species comparison showed that a cell type similar to ABPCs is present in mouse regenerative digit tip (P3) but not in mouse nonregenerative digit tip (P2), axolotl limb, or zebrafish caudal fin. This suggests the existence of relatively conserved cellular and molecular mechanisms for the only two known cases of regenerative capacity in mammalian appendage organs.

Our in vitro and in vivo results suggest that deer ABPCs may have an application in clinical bone repair. Beyond this, induction of regular human mesenchymal or other cells into ABPC-like cells through activation of key characteristic genes could potentially be used in regenerative medicine for skeletal injuries or limb regeneration.

### REFERENCES AND NOTES

- 1. J. A. Goldman, K. D. Poss, Nat. Rev. Genet. 21, 511-525 (2020).
- 2. T. Gerber et al., Science 362, eaaq0681 (2018)
- 3. Y. Hou et al., Sci. Adv. 6. eaba2084 (2020).
- 4. J. Godwin, BioEssays 36, 861-871 (2014).
- J. P. Brockes, A. Kumar, Nat. Rev. Mol. Cell Biol. 3, 566–574 (2002).
- S. E. Iismaa et al., NPJ Regen. Med. 3, 6 (2018).
- 7. R. J. Goss, Anat. Rec. 241, 291-302 (1995).
- C. Li, H. Zhao, Z. Liu, C. McMahon, Int. J. Biochem. Cell Biol. 56, 111–122 (2014).
- U. Kierdorf, H. Kierdorf, T. Szuwart, J. Morphol. 268, 726–738 (2007).
- J. S. Price, S. Allen, C. Faucheux, T. Althnaian, J. G. Mount, J. Anat. 207, 603–618 (2005).
- 11. T. Landete-Castillejos et al., Bone 128, 115046 (2019).
- C. Li, J. M. Suttie, D. E. Clark, Anat. Rec. A Discov. Mol. Cell. Evol. Biol. 282A, 163–174 (2005).
- 13. C. Li, J. M. Suttie, D. E. Clark, J. Morphol. 262, 731-740 (2004).
- 14. Y. Wang et al., Science 364, eaav6335 (2019).
- Materials and methods are available as supplementary materials.

- 16. T.-Y. Lin et al., Dev. Cell 56, 1541-1551.e6 (2021).
- 17. G. L. Johnson, E. J. Masias, J. A. Lehoczky, *Dev. Cell* **52**, 525–540.e5 (2020).
- 18. C. Li, Birth Defects Res. C Embryo Today 96, 51-62 (2012).
- D. E. Clark, C. Li, W. Wang, S. K. Martin, J. M. Suttie, *Anat. Rec. A Discov. Mol. Cell. Evol. Biol.* 288A, 973–981 (2006).
- J. W. Godwin, A. R. Pinto, N. A. Rosenthal, *Proc. Natl. Acad. Sci. U.S.A.* 110, 9415–9420 (2013).
- 21. A. W. Seifert, K. Muneoka, Dev. Biol. 433, 190-199 (2018).
- 22. M. A. Storer et al., Dev. Cell 52, 509-524.e9 (2020).
- 23. H. Li et al., Protein Cell 12, 57-66 (2021).
- 24. A. Arthur, S. Gronthos, Int. J. Mol. Sci. 21, 9759 (2020).
- N. H. Kelly, N. P. T. Huynh, F. Guilak, *Matrix Biol.* 89, 1–10 (2020).
- L.-A. Stanton, T. M. Underhill, F. Beier, Dev. Biol. 263, 165–175 (2003).
- E. Kozhemyakina, A. B. Lassar, E. Zelzer, *Development* 142, 817–831 (2015).

### **ACKNOWLEDGMENTS**

We thank P. Fennessy for critical reading of the manuscript and Jilin Dong Ao Deer Industry Group Co. for providing deer antler

samples. We also thank Z. Wang, Q. Guan, J. Li, S. Wang, and D. Wang from the Institute of Antler Science and Product Technology for their help in single-cell separation. Funding: This study was supported by the National Key Research and Development Program of China (grant 2021YFA0805000), the National Natural Science Foundation of China (grants 32225009, 31970392, 82122043, 32030016, 32122083, and U20A20403), the Strategic Priority Research Program of the Chinese Academy of Sciences (grant ref. XDA16010105), the Talents Team Construction Fund of Northwestern Polytechnical University, the Research Funds for Interdisciplinary Subject (grant NWPU 19SH030408), and the 1000 Talents Project of Shaanxi Province. Author contributions: Q.Q., C.L., J.H., and W.W. designed this project and research aspects. Z. Li, Q.L., H.S., T.Q., Z. Liu, and G.Z. performed sample collection and sequencing library construction. M.H. and Y.Y. performed data analysis including genome assembly and annotation. S.L. and Y.Z. performed flow cytometry. Y.Z., S.L., G.W., G.Z., X.C., J.R., B.X., H.B., and X.G. performed functional experiments. T.Q. and Y.Y. performed scRNA-seq analysis. K.W., G.W., and T.Q. contributed to figure design. T.Q., Q.Q., W.W., Z. Li, and J.H. wrote the manuscript. W.W. and R.H. amended it. Competing interests: Q.Q., J.H., T.Q., Y.Z., and W.W. are inventors on a patent application related to this work filed by Northwestern Polytechnical University and Fourth Military Medical University (patent application no. CN202211737365.3). 

Data and materials availability: All sequencing data and genome assemblies have been deposited in the NCBI database (accession ID: PRJNA831044). All other data needed to evaluate conclusions in the paper are present in the paper and/or supplementary materials. Additional data related to this paper may be requested from the authors. License information: Copyright © 2023 the authors, some rights reserved; exclusive licensee American Association for the Advancement of Science. No claim to original US government works. https://www.science.org/about/science-licenses-journal-article-reuse

#### SUPPLEMENTARY MATERIALS

science.org/doi/10.1126/science.add0488 Materials and Methods Figs. S1 to S11 Tables S1 to S11 References (28–54) MDAR Reproducibility Checklist

Submitted 17 May 2022; resubmitted 16 November 2022 Accepted 10 January 2023 10.1126/science.add0488

Qin et al., Science **379**, 840–847 (2023) 24 February 2023 **8 of 8**